Shahrood University of Technology

Journal of Mining and Environment (JME)

Journal homepage: www.jme.shahroodut.ac.ir

Iranian Society of Mining Engineering (IRSME)

Effect of Tunnel Location Related to Inclined Coal Strata on Excavation-Induced Displacements of Mine Tunnel: Application of Calibrated Numerical Model

Morteza Javadi[1]*, Ashkan Shahpasand[1], Shahrbanou Sayadi[2], and Arash Shahpasand[3]

1. Faculty of Mining, Petroleum & Geophysics Eng., Shahrood University of Technology, Shahrood, Iran
2. Faculty of Mining Engineering, Isfahan University of Technology, Isfahan, Iran
3. Tehran Science and Research Branch Islamic Azad University., Iran

Article Info

Received 15 January 2023
Received in Revised form 17 July 2023
Accepted 14 August 2023
Published online 14 August 2023

DOI: 10.22044/jme.2023.12611.2291

Keywords

Stratified Rock Mass
Coal Mine
Numerical Model
Monitoring-based Calibration
Asymmetric Displacements

Abstract

The stratified-sedimentary rock mass, as the typical host ground of coal mine tunnels, is characterized by highly non-isotropic deformation due to the very persistent discontinuity of bedding planes. This study evaluates the effect of tunnel location relative to the host ground strata on the excavation-induced displacements around a coal mine tunnel driven along the inclined coal seam. To achieve this goal, a calibrated finite element method (FEM) numerical model based on field monitoring displacements was developed for the coal mine tunnel at a depth of 300 m. This calibrated numerical model was then utilized to investigate the effect of the horizontal location of the tunnel on the induced displacement field through sensitivity analysis. Finally, the sensitivity analysis results were compared in terms of displacement components around the tunnel. The results of this study demonstrate a reasonable level of accuracy (for practical demands) of the calibrated numerical model, with an average error of about 8% for maximum displacements at measured points. The numerical models show an asymmetric spatial distribution of displacements around the tunnel due to the anisotropy of the rock mass, especially in the case of inclined layers. The arrangement of weak-strength coal and intercalary stone layers relative to the excavation line of the tunnel plays a key role in this issue. The critical state of displacements (maximum displacement in sensitivity analysis) occurs where the intersection line of the coal-intercalary stone is tangent to the tunnel excavation line. Additionally, the excavation-induced displacement decreases as the distance between the coal-intercalary stone interface and the tunnel increases, with a distance of about 1.5 m suggested for practical applications.

1. Introduction

Stratified rock mass is a common host medium in mining and civil engineering, where excavation in sedimentary rock is attempted. The most relevant feature of stratified rocks is the occurrence of very persistent discontinuities, or bedding planes, which make the rock mass highly non-isotropic. The anisotropy of the mechanical characteristics of stratified rocks mainly consists of rock strength, failure mode, and deformation, which are associated with the dip angle between the axial loading direction and the normal of the weak plane [1]. These characteristics control the interaction between the host ground and underground excavations. Therefore, the characterization of such behavior is very important for the economic design and safe construction of underground excavations.

The structure of a stratified rock mass plays a vital role in the mechanical behavior of an underground opening during excavation and operation [2]. When a tunnel is excavated in stratified ground, especially in lithologically varied sedimentary rock masses, the stress and deformation characteristics of the surrounding rock mass are very different from those in normal rock masses [3]. Therefore, designing a tunnel through

Corresponding author: mortezjavadi@gmail.com (M. Javadi)

stratified host rock requires the consideration of a variety of different mechanisms, since the rock mass exhibits a wide spectrum of behavior depending on intact rock and rock mass properties, in-situ stresses, and the relative direction of stratification with respect to the tunnel section [4]. Obviously, the assessment of excavation stability in such a host medium is much more complex, as it is often associated with factors that lead to highly anisotropic behavior of the rock mass [3,5]. To achieve proper design and construction in this situation, it is necessary to properly analyze the effects of heterogeneity and anisotropy. Many researchers have focused on the behavior of stratified rock masses, either to recognize the pure overall mechanical behavior of the medium or to study its response to excavation. The investigation approaches of these studies mainly consist of experimental methods, theoretical analysis, field experiments, physical model testing, and numerical simulation. Most of the experimental studies [6-8] have focused on the mechanical behavior of stratified media in the absence of excavation. However, these types of studies cannot be directly applied to properly evaluate the interaction of the rock mass and underground excavation. Theoretical models [9-14] can reflect the main principles of rock mass behavior, but are limited to very simple geometries of underground excavations. Furthermore, it is impossible to explore all mechanical characteristics by implementing a theoretical model. Field experiments [15-17] and physical model testing [18-22] can be introduced as alternative methods to overcome the limitations of theoretical models. However, these methods can be expensive and time-consuming, and may encounter scale effect problems. In fact, full-scale physical modeling experiments are very expensive and difficult to operate. On the other hand, small-scale tests are limited by the size of the model and may be inefficient in realistically simulating in-situ stresses. Considering the limitations involved in using the above methods, numerical techniques have proven to be essential and powerful tools in modeling stratified rock masses [23-33]. The finite element method (FEM) is one of the most common methods in the continuum modeling approach, which assumes the rock mass as a continuous material and analyzes the mechanical performance of intact rock and rock properties [34]. Numerical methods have been considered more suitable for simulating the rock mass response in different geo-mechanical fields, especially for stratified surrounding rock around tunnels. However, few studies have focused on the effect of inclined stratification on the stability of non-circular excavations with respect to the location of rock layers. To the best of the authors' knowledge, most previous research has either focused on investigating the behavior of circular tunnels considering the influence of inclined stratification [4, 26] or the behavior of non-circular tunnels excavated in horizontal stratification [35]. So far, with the exception of one case [25], which studied the effect of bedding dip angle on non-circular excavation stability, the role of the horizontal location of excavation surrounded by inclined bedding on the induced displacement field has not been investigated. This issue forms the main contribution of this study.

This study aims to investigate the effect of inclined beddings and the location of excavation with respect to different ground strata on the displacement field developed around a non-circular tunnel by applying a calibrated numerical model. To achieve this goal, a reference numerical model was adopted based on the back analysis results of field monitoring measurements. The calibrated model was then used to investigate the appropriate horizontal location of the tunnel through sensitivity analysis. In this analysis, the induced displacement components around the tunnel were evaluated for different locations. Finally, the results from different numerical models were compared to find the most suitable location for the tunnel.

2. Theory and Background

While the demand for minerals and metals continues to grow rapidly, underground mining operations are progressing into deeper and increasingly complex deposits associated with more challenging geological conditions. Coal resources are typical reservoirs found in sedimentary strata sequences. Extraction of these resources requires the majority of mining tunnels to be driven in these strata, where the mechanical behavior often varies from one layer to another, even within a closely related geological sequence. Generally, tunneling may induce significantly different magnitudes of deformation in the surrounding ground. In terms of layered strata, excavation of a tunnel removes the confinement on the surface of the profile and induces a stress concentration zone around the tunnel, disturbing and destroying the original equilibrium condition. The disequilibrium in the stress field triggers deformation and closure of the tunnel. Furthermore, the thickness and material of the variable rock layers may affect the stability of the excavated tunnel/adit, which arises from the layered nature of the coal resource. This is why in engineering practice, it has been proven that rock anisotropy and heterogeneity are important factors in stabilizing underground excavations in layered rock masses such as coal [4, 36].

Generally speaking, the structure of a stratified rock mass plays a vital role in the mechanical response of an underground opening during excavation and operation. Therefore, the reference stratified rock mass can be considered as the qualitative sum of the internal rock mass and the dominant discontinuities. However, there are often significant differences between the mechanical parameters of the reference stratified rock and the actual rock mass, so it is recommended to adjust the rock mass properties accordingly [37-39]. Assuming that the rock mass is a combination of intact rock and discontinuities, the deformability properties of these elements can be calculated using the following equations [40, 41]:

$$\frac{1}{E_{m,ref}}=\frac{1}{E_{m,int}}+\frac{1}{s_p k_n} \quad (1)$$

$$\frac{1}{G_{m,ref}}=\frac{1}{G_{m,int}}+\frac{1}{s_p k_s} \quad (2)$$

where $E_{m,ref}$ and $G_{m,ref}$ are the reference rock mass deformation and shear modulus, $E_{m,int}$ and $G_{m,int}$ the deformation and shear modulus of the internal rock mass between discontinuities, s_p is the spacing of discontinuities (or bedding thickness), k_{nn} and k_{ss} the normal and shear stiffness of the discontinuities, respectively. The deformation modulus of the internal rock mass ($E_{\mathrm{m,int}}$) is calculated based on the following relationship [39]:

$$E_{m,int}=E_i\left[0.02+\frac{1-{}^{D}/_{2}}{1+e^{(60+15D-GSI)/11}}\right] \quad (3)$$

where D is the disturbance factor and E_{i} is the deformation modulus of initial rock, which is determined by the formula [39]:

$$E_i=MR\sigma_{ci} \quad (4)$$

The shear modulus of and internal rock mass ($E_{\mathrm{m,int}}$) and initial rock (G_{i}) can be estimated by formulas:

$$G_i=\frac{E_i}{2(1+\mu)} \quad (5)$$

$$G_{rm}=\frac{E_{rm}}{2(1+\mu)} \quad (6)$$

where μ is Poisson's ratio of the rock mass.

3. Case Study and Model Setup

3.1. Case description

This paper investigates the stress and displacement field around a non-circular excavation that was driven along a coal seam. The study is based on the N-6-8 tunnel in the Duonghuy coal mine, Quang Ninh, Vietnam [25]. The tunnel was excavated along a coal seam (Fig. 1) in order to exploit the coal and transport it to the outside. As illustrated in Fig. 1, the excavation cross-section is assumed to be a modified-horseshoe with vertical sidewall dimensions of 4 m wide and 3.25 m height, located at a depth of 300 m below the ground surface. To reduce the complexity of the numerical modeling analysis and make it computationally feasible, the conditions of pore-water pressure in the rock and rock mass are assumed to be "dry" or undrained.

The stratified rock mass in the Quang Ninh coal mine consists of conglomerates, quartz siltstone, and sandstone interbedded with thin layers of intercalary stone and coal seams. A range of Geological Strength Index (GSI) values that range from 10 to 80 has been adopted to cover rock mass conditions that vary from very poor to very good. The GSI values, deformability, and strength parameters of the rock masses (calculated based on the theoretical and empirical equations in the previous section) are presented in Table 1. The uniaxial compressive strength of intact rock (σ_{ci}) ranges from 20 MPa to 86 MPa, with a modulus ratio (MR) of 500 and a geomaterial constant (m_i) of 7. The strength parameters of the discontinuities (interfaces between rock layers) are based on the surface quality of the reference rock mass. The Joint Roughness Coefficient (JRC) values range from 2 (very poor) to 18 (very good), and the Joint Compressive Strength (JCS), calculated as a fraction of the intact rock uniaxial compressive strength (σ_{ci}), varies from 0.10σ_{ci} (very poor) to 0.60σ_{ci} (good). The interface properties of the internal rock masses are also summarized in Table 2.

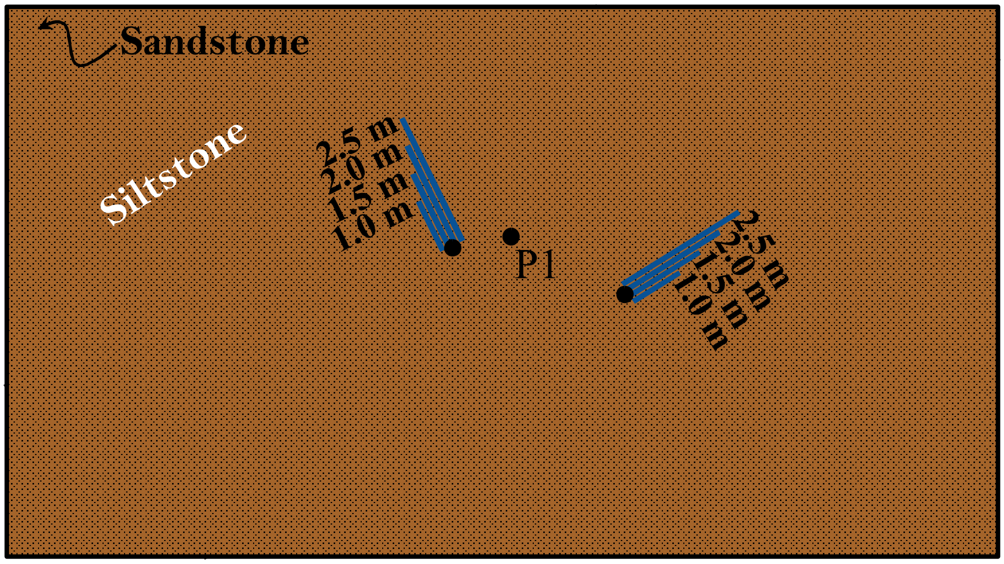

Figure 1. Cross-section of tunnel in inclined stratification ground and detail of monitoring extensometers installed in the tunnel (modified based on the [25]).

Table 1. Initial and calibrated geo-mechanical parameters of rock layers surrounding the tunnel.

Layer	Density(g/cm^3)	E(Mpa)		GSI	σ_{ci}(Mpa)	c(MPa)	φ(°)
		Initial	Calibrated				
Sandstone	2.65	11585	8024	60	86.62	1.33	40.59
Siltstone	2.65	4772	2470	50	46.48	0.69	31.95
Coal	1.4	556	490	20	20	0.19	14.23
Intercalary Stone	2	2624	2186	45	25	0.39	27.34

Table 2. Interface properties of the internal rock mass surrounding the tunnel [25].

Rock in contact	JCS (MPa)	JRC
Sandstone-Siltstone	23.24	10
Siltstone-Intercalary Stone	7.5	6
Intercalary Stone-Coal	2	2
Coal-Siltstone	2	2

To obtain the deformation characteristics of the induced displacements in the rock mass after excavation, three extensometers were installed in the rock mass from the tunnel wall. Two shoulders of the arch and the roof were selected for installing four-rod extensometers with different lengths of 1 m, 1.5 m, 2 m, and 2.5 m. The layout of the monitoring points is shown in Figure 1. The displacements induced in the rock mass were frequently monitored for six months until the tunnel boundary reached a stable state. During construction, the tunnel was supported by steel ribs to ensure the equilibrium and stability of the tunnel. The structural properties of the steel ribs used for tunnel support are summarized in Table 3. It should be noted that the steel ribs were installed at a maximum distance of 0.7 m from the tunnel face immediately after each excavation.

Table 3. Structural properties of steel ribs used for tunnel support [25].

Height of section (m)	Cross-sectional area (m^2)	Inertia moment (m^4)	Young's modulus (GPa)	Poisson's ratio
0.171	0.002173	2.43×10^{-6}	180	0.25

3.2. Numerical model setup

Numerical analyses in plane strain were conducted using the finite element code Phase2. This software uses an implicit finite element method for plasticity analysis, employing Newton-Raphson solution schemes, which are iterative procedures that have been shown to be the most robust and economical scheme in terms of computing time [42]. Different numerical models including the initial model, back-calibrated model, and sensitivity analysis models were used for investigation purposes. The initial model was used to evaluate the numerical model and compare the results with monitoring data. Based on this comparison, the initial model was calibrated for the next analysis. After calibrating the geo-mechanical properties of the rock strata and interfaces, a sensitivity analysis was performed by horizontally shifting the tunnel relative to the coal seam to find the most stable configuration.

In all of the numerical models, the horseshoe tunnel section was simulated in a numerical model measuring 25 m x 25 m (approximately six times the tunnel dimension) to avoid the effects of boundaries. This numerical domain represents the tunneling-affected domain with artificial boundaries, and the effect of in-situ stress was numerically applied to the models. The arrangement of rock strata was adopted based on geological explorations conducted in the monitoring section, as shown in Figure 2. This relative location of the tunnel and rock strata, referred to as the geological-tunnel configuration, was considered the reference section or original model (hereafter named "OM"). The rock mass was quantified using the Hoek–Brown failure criterion [43], the discontinuity strength was evaluated using the Barton-Bandis failure criterion [44], and the rock mass deformation modulus was calculated based on the relationship proposed by Hoek and Diederichs (2006) [39]. The internal rock mass and discontinuity parameters for the initial model are presented in Tables 1 and 2 (calculated based on the procedure described in the previous section). The parameters were assigned to the various strata in the numerical models. The normal fixed boundary condition was applied to the numerical model boundaries, as is typically suggested for artificial domain boundaries. In fact, the boundary condition for the numerical models is fixed in all directions on the parallel and normal directions of the boundary sides. Graded six-noded triangular elements with a gradation factor of 0.1 were utilized to mesh the numerical domain. The boundary condition, tunnel size, domain size, and mesh details of the numerical model for the reference section (OM) are shown in Figure 2. For all numerical models, a dense mesh was used in and around the tunnel, whereas a coarser mesh was used for the areas farther away from the tunnel. The first step in the numerical modeling process consisted of setting up the initial stress state, considering the vertical stress under the effect of the gravity field. Since the numerical domain represents a limited area surrounding the tunnel, the effect of the overburden stress (associated with a tunnel depth of 300 m) was indirectly applied through vertical and horizontal extra stresses on the model boundaries. In all the numerical models, the ratio between lateral and vertical stresses (K0) was assumed to be 0.5, based on the back-analysis results from a previous study.

This study involved different numerical analyses that were performed based on specific requirements. These analyses can be categorized as follows:

a) Establishing the initial model based on the empirical assumed properties of the tunnel and surrounding reference rock mass and comparing results with monitoring measurements;

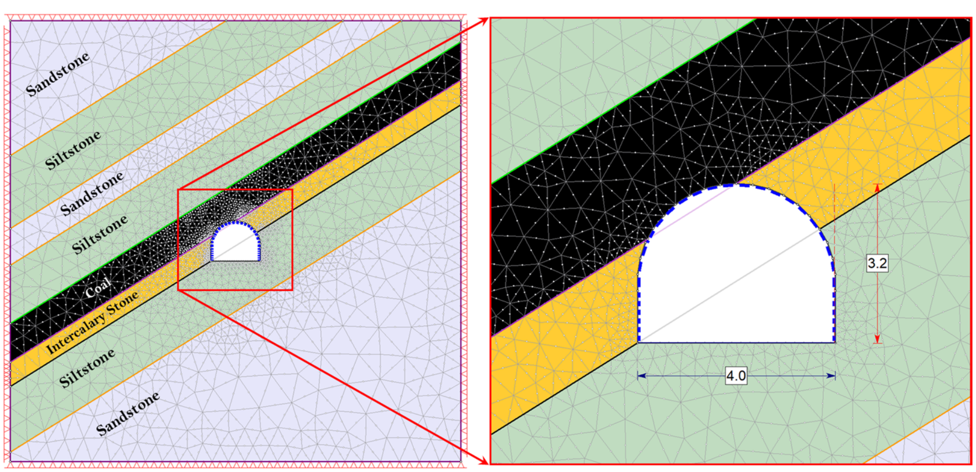

Figure 2. Numerical model for reference section (OM) with the arrangement of rock strata, boundary conditions, and numerical mesh.

b) Calibrating the initial model through back analysis on the geo-mechanical parameters of the surrounding rock mass to adjust the numerical model results with monitoring measurements;

c) Implementing the calibrated model to analyze the effect of tunnel horizontal location on induced deformation and stress field around the tunnel to select the appropriate location of the tunnel as a demand of design optimization.

In order to validate the simulation results, the reference numerical model has been established based on the geo-mechanical parameters obtained from empirical approximations. Then the geo-mechanical parameters of the reference model were calibrated based on the results of monitoring measurements to increase the accuracy of the numerical simulation. These analyses were performed on the OM reference section. Finally, the calibrated model has been used to determine the appropriate location of the tunnel relative to the coal layer as a design optimization demand. For this purpose, numerical modeling of tunnel-induced displacements has been carried on for eight different locations relative to the initial tunnel location. A schematic view of the tunnel location transition relative to the initial location is illustrated in Fig.3. The location of the tunnel is shifted with intervals of 50 cm horizontally to the left and right (resulting in decreasing and increasing the distance from the coal layer, respectively) that resulted to eight different study cases for sensitivity analysis. Each model was numerically analyzed individually.

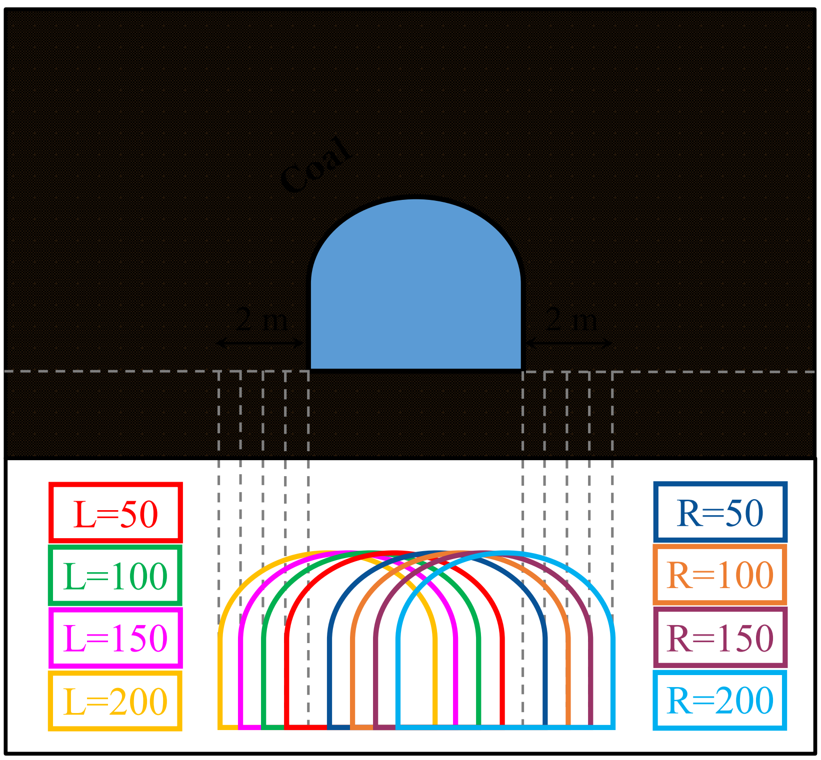

Figure 3. Schematic view of the horizontal transition of tunnel location relative to the initial location (dislocation at distances of every 50 cm to the right and left).

4. Results and Discussion

The initial analysis of the interaction between the rock strata and tunnel was performed based on a numerical model with geo-mechanical parameters derived from the empirical equation presented in Table 1. The total net displacement induced by the tunnel excavation (as measured by the monitoring system) is shown in Figs. 4-a and 4-b, with the displacement at the installed extensometer points marked in Fig. 4-b. These results indicate that a net total deformation in the range of 0 to 100 mm arises around the tunnel after excavation and support installation. Based on the initial numerical model results, the net total deformations at the extensometer points are estimated to range from 10 mm to 20 mm, 10 mm to 20 mm, and 0 to 5 mm for P1, P2, and P3 extensometers, respectively. However, the measured deformations at these points range from 15 mm to 95 mm, indicating inadequate precision of the initial model corresponding to the measured values obtained by the monitoring system. Therefore, calibration of the numerical model is necessary to increase its accuracy, especially for sensitivity design analysis.

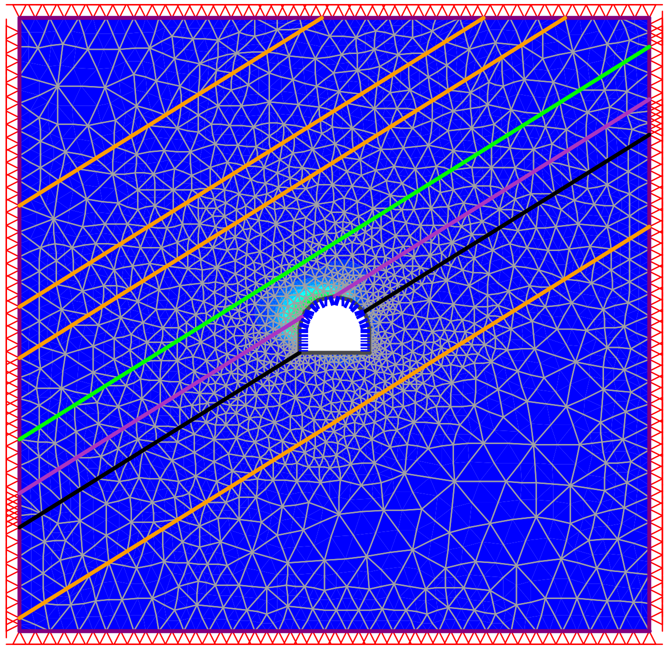

a) Full scale the tunnel excavation

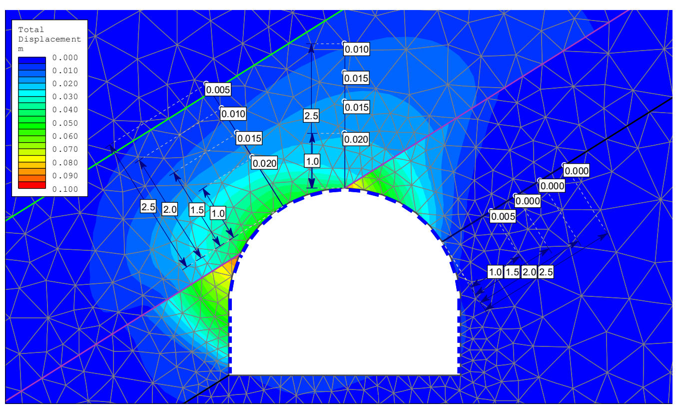

b) Total net displacement-monitoring system

Figure 4. Total net displacement after tunnel excavation and support for initial numerical model: Full scale the tunnel excavation (a), and Total net displacement-monitoring system (b) (for the OM reference section).

In To increase the accuracy of the analysis, the numerical model for the OM reference section was calibrated by minimizing the discrepancy between the measured displacement (derived from monitoring results) and the corresponding numerically evaluated quantities using the multi-variable direct method for back analysis. The displacement values at the corresponding extensometer points, estimated by the back-calibrated numerical model, as well as the measured values obtained from the monitoring instruments, are summarized in Table 4. To better evaluate the validity of the estimates, the results of a previous study conducted on this tunnel case (Do *et al.*, 2019 [25]) are also presented in Table 4.

Table 4. Comparison between displacements in corresponding points of extensometers estimated by the back-calibrated numerical model and measured values by the monitoring instruments.

		Displacement in rock mass (m)								
		Measured data [25]			Previous Study [25]			This study		
Extensometer ID		P1	P2	P3	P1	P2	P3	P1	P2	P3
Distance from the tunnel wall (m)	1	0.08	0.095	0.015	0.06	0.088	0.012	0.067	0.093	0.014
	1.5	0.045	0.09	0.015	0.047	0.066	0.008	0.042	0.067	0.008
	2	-	0.04	0.015	0.033	0.045	0.008	0.03	0.039	0.008
	2.5	0.02	0.04	0.015	0.027	0.028	0.008	0.02	0.029	0.008
Maximum displacement (D_{max})		0.08	0.095	0.015	0.06	0.088	0.012	0.067	0.093	0.014
D_{ratio}*		-	-	-	0.75	0.93	0.8	0.84	0.98	0.93

* The displacement ratio (D_{ratio}) is obtained by dividing the maximum displacement of the model by the maximum displacement measured as $D_{ratio} = D_{max-model}/D_{max-measured}$.

According to Table 4, there are slight discrepancies between the estimated results of the calibrated model and the field-measured displacements, but there is still an acceptable level of consistency between the results. To highlight this consistency, a factor used for comparing the calibrated model and measured values is introduced as D_{ratio}. This parameter represents the ratio of the maximum displacements at a specific point in the calibrated model to the same point measured by monitoring in the tunnel. As D_{ratio} approaches one, it indicates a proper estimate of the numerical model. According to Table 4, the D_{ratio} values at P1, P2, and P3 are 0.84, 0.98, and 0.93, respectively. The estimate error for P1 is the highest at about 16%, whereas the errors for P2 and P3 are only 2% and 7%, respectively. This comparison indicates the overall accuracy of the calibrated numerical model.

The distribution of stress and deformation around the tunnel is one of the most important outputs of the numerical model, which can be used to inform design decisions and planning alternatives. The output results of the calibrated numerical model for the OM reference section are shown in Fig. 5, in terms of principal stresses and deformation around the tunnel. The contour plot and trajectory of principal stresses (Figs. 5-a and 5-b) reveal a complete asymmetrical state around the tunnel. The trajectory of principal stresses indicates that the excavation-induced stresses are mainly deviated from the internal boundary control state. This behavior becomes more evident at the crown of the tunnel, where it is usually expected that the axis of major and minor principal stresses will be parallel and perpendicular to the excavation line of the tunnel, respectively. In fact, the direction of principal stresses around the tunnel is mainly controlled by the inclination of the rock strata rather than the shape of the tunnel boundary. The deviation of the principal stress direction from symmetry can be clearly observed in the upper-right side area around the tunnel (in the coal and intercalary stone strata). Furthermore, the values of both major and minor principal stresses in this area are lower than those in other areas around the tunnel due to the weaker strength of the coal and intercalary stone strata. Similarly, the displacement induced by tunnel excavation shows an asymmetric distribution around the tunnel. The horizontal displacements are mainly concentrated on the left side of the tunnel (Fig. 5-c). In addition, intense vertical deformation can be seen on the left side of the tunnel crown area (Fig. 5-d). The spatial distribution of excavation-induced deformation is clearly controlled by the location of the weak strength coal and intercalary stone strata. The presence of inclined weak layers around the tunnel is the main reason for the asymmetric deformation distribution that reflects the anisotropy of the rock mass behavior. Under such conditions, the location of weak strata relative to the tunnel plays a crucial role in the induced stress and deformation around the tunnel. This issue will be further discussed in the rest of the study.

Sensitivity analysis was conducted to investigate the effect of the horizontal location of the tunnel relative to the host ground layers on induced deformations around the underground excavation. In this regard, eight horizontal locations were considered by transitioning the tunnel's initial location (OM) to the left (toward the coal layer) and to the right (away from the coal layer), based on the schematic view shown in Fig. 3. The results of the sensitivity analysis are presented in Figs. 6 to 8, in terms of the absolute horizontal, absolute vertical, and total displacements induced by tunnel excavation and support, respectively. These figures show the corresponding transmitted locations to the left, which are marked as L50, L100, L150, and

L200, and to the right, which are marked as R50, R100, R150, and R200. Additionally, the reference section is marked as OM. It is important to note that, for each shifted tunnel location, numerical modeling was performed while keeping the geomechanical parameters, geological configuration, numerical setup, and boundary conditions constant.

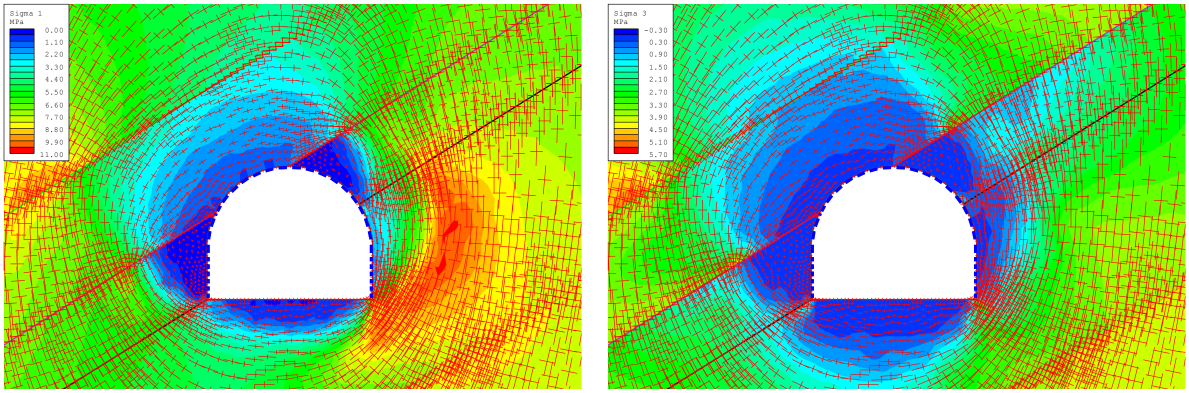

a) Major principal stress (σ_1) **b) Minor principal stress (σ_3)**

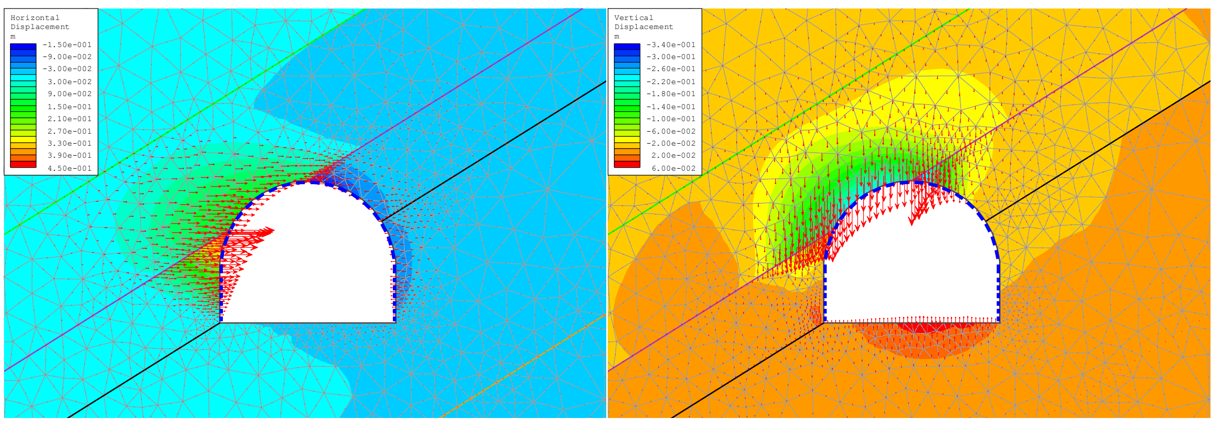

c) Horizontal displacement **d) Vertical displacement**

Figure 5. Output results of calibrated numerical model: contour plot plus trajectory of principal stress (a, b), and contour plot plus the displacement vectors (c, d).

The contour plots of absolute horizontal displacement around the tunnel for the sensitivity analysis of tunnel horizontal location are shown in Fig. 6. This figure illustrates the effect of the tunnel's horizontal location on the induced horizontal displacements. The horizontal displacement induced by tunnel excavation shows an asymmetric spatial distribution around the tunnel. It is evident that the arrangement of weak strength coal and intercalary stone strata relative to the tunnel excavation line plays a key role in the asymmetric spatial distribution of excavation-induced horizontal deformation. In fact, the anisotropy of rock mass behavior due to the inclined weak layers is associated with the asymmetric spatial deformation distribution. For most cases, the majority of horizontal displacement occurs at the intersection area of the coal-intercalary stone interface with the excavation line of the tunnel.

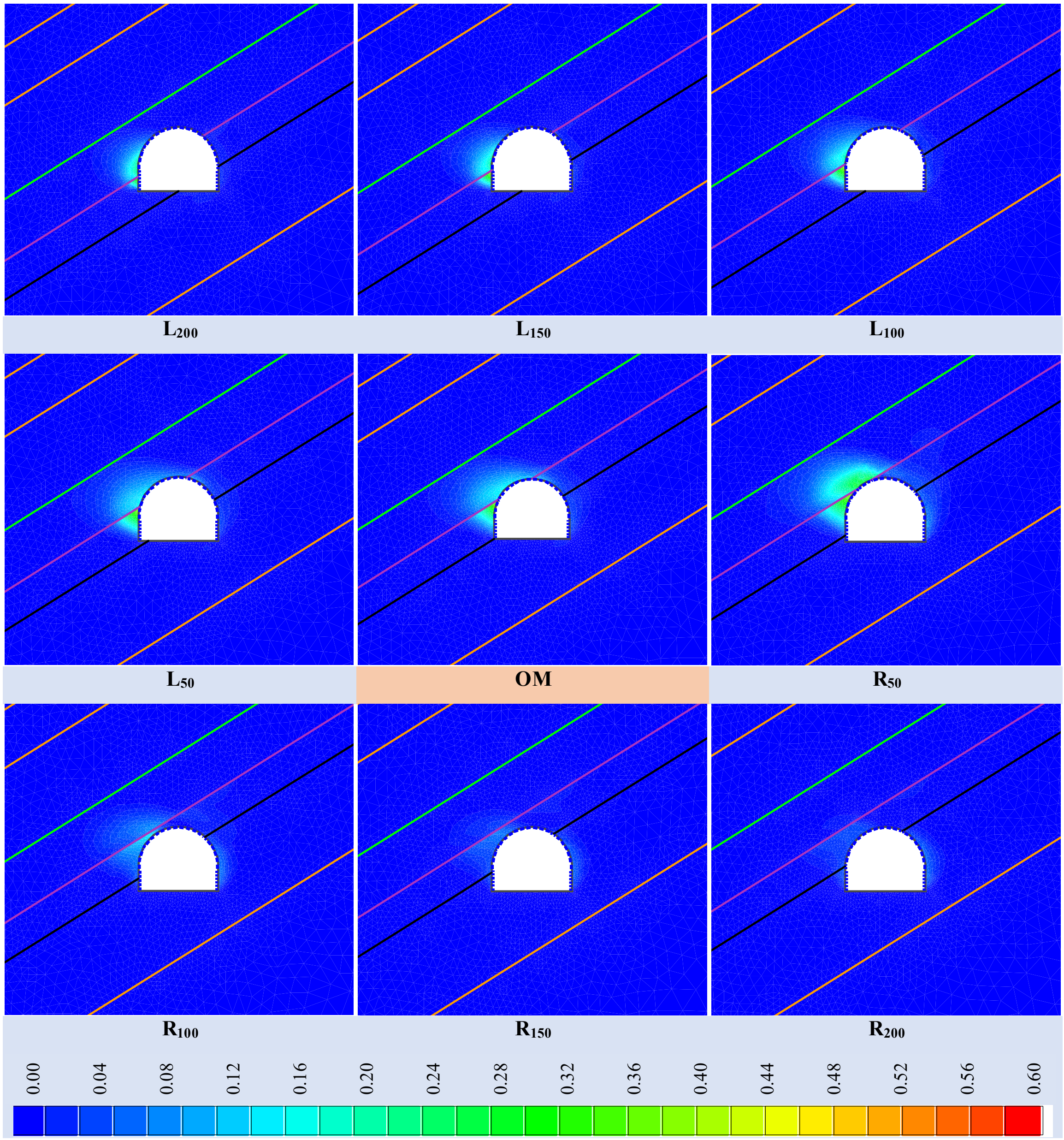

Figure 6. Contour-plot of absolute horizontal displacements around tunnel induced by excavation for different tunnel horizontal locations relative to OM reference section.

As shown in Fig. 6, the horizontal displacement gradually increases as the horizontal distance decreases from left to right (from L_{200} to OM). For these horizontal locations of the tunnel, most of the horizontal displacements occur at the left sidewall of the tunnel. The concentration area of displacements moves upward from the left sidewall to the crown of the tunnel by shifting the horizontal distance from L_{200} to OM. Abrupt changes in the spatial distribution and value of horizontal displacement can be found at the tunnel horizontal location of R_{50}. At this location, the induced horizontal displacements extend to a larger area around the left sidewall and crown of the tunnel, and the value of horizontal displacement reaches its maximum. A distinguished reduction in horizontal displacement is observed when the tunnel transitions from R_{50} to R_{100}. The horizontal displacement slowly decreases as the tunnel shifts to the right from R_{100} to R_{200}. In this situation, the cases of R_{150} and R_{200} show the minimum horizontal displacement induced by tunnel excavation.

Fig. 7 shows the contour plots of vertical displacement induced by excavation. This figure illustrates the effect of the tunnel's horizontal location on the induced vertical displacement as a result of sensitivity analysis. For all horizontal locations, most of the vertical displacements around the tunnel are concentrated in the left half of the tunnel area, creating an asymmetric vertical displacement field. The asymmetrical intensity of the spatial distribution of vertical displacements is much more noticeable for the R_{50} and OM cases. The magnitude and spatial spread of the induced vertical displacement increase gradually as the tunnel horizontal location is shifted from L_{200} to R_{50}. For the other cases of R_{100}, R_{150}, and R_{200}, the magnitude and spatial spread of the induced vertical displacement decrease as the tunnel is shifted to the right. Hence, the magnitude and spatial spread of the induced vertical displacement reach their maximum for the R_{50} case. Additionally, the minimum magnitude and spatial spread of the induced vertical displacement occur in the case of R_{200}.

The numerical analysis results also show a particular type of vertical displacement at the tunnel floor. The numerical model for all horizontal locations of the tunnel displays uplift vertical displacement or heave of the tunnel floor, as shown in Fig. 7. The magnitude of floor heave for tunnel locations on the left side (L_{50}, L_{100}, L_{150}, and L_{200}) is much higher than those on the right side (R_{50}, R_{100}, R_{150}, and R_{200}). In addition, the magnitude of floor heave for both left and right side tunnel locations shows very low dependency on the horizontal movement of the tunnel. The change in the magnitude of floor heave only occurs in the area of the floor where there is a change in the strata type. This change in floor strata type occurs at the OM section, where the tunnel floor of the left side horizontal location consists of two types of strata, including siltstone and intercalary stone, while the tunnel floor of the right side models is located on the siltstone layer. Since the intercalary stone has weak mechanical properties, a greater magnitude of floor heave is anticipated for the left side location of the tunnel (L_{50}, L_{100}, L_{150}, and L_{200}), as predicted by the numerical models.

The contour plots of total displacement, shown in Fig. 8, illustrate the effect of tunnel horizontal location on the induced deformation caused by tunnel excavation. Total displacement around the tunnel is the sum of individual displacement components. As such, it can serve as a suitable measure for interpreting sensitivity analysis results. Based on the results of Fig. 8, the effect of horizontal movement of the tunnel location on induced deformations can be spatially interpreted. The spatial spread of the affected area by total displacement increases as the horizontal distance decreases from left to right for these cases. At the tunnel horizontal location of R_{50}, sudden increases of total displacement occur, indicating the maximum magnitude and spread of total displacement induced by tunnel excavation. The magnitude and spatial spread of induced total displacement decrease, especially with an increase in right-side movement of tunnel horizontal location for cases of R_{100}, R_{150}, and R_{200}. Therefore, the case of R_{200} exhibits the minimum magnitude and spatial spread of induced total displacement.

Similar to the vertical and horizontal displacement components, the total displacement field around the tunnel in inclined stratified strata exhibits an asymmetric spatial distribution. As shown in Fig. 8, the induced total displacements are concentrated in the area where the coal-intercalary stone interface intersects with the tunnel excavation line. The magnitude, shape, and spatial distribution of induced total displacements around the tunnel are controlled by the spatial location of these weak rock strata relative to the tunnel boundary. Therefore, decreasing the proximity of the coal and intercalary stone layers to the tunnel boundary or reducing the excavation area of these weak layers (coal and intercalary stone) can decrease both the magnitude and spatial spread of induced total displacement.

To precisely investigate the effect of tunnel location on induced deformations, we studied the variation of displacement components along different tunnel locations using quantitative graphs. In this regard, five observation points were considered at the tunnel boundary. The location of the observation points on the tunnel boundary and the resultant displacement components on these points are shown in Fig. 9. In this figure, the displacement components induced by excavation in terms of absolute horizontal, absolute vertical, and total displacements were derived from the results of numerical models and plotted as a function of tunnel horizontal distance of OM section. It should be noted that the horizontal axis (X-axis) of graphs in Fig. 9 shows the value of horizontal distances of tunnel relative OM section, where the left and right side transition of tunnel are indicated as negative and positive values, respectively. In other words, the values of L_{50}, L_{100}, L_{150}, and L_{200} cases on the x-axis are -50, -100, -150, and -200, respectively. Similarly, the values of R_{50}, R_{100}, R_{150}, and R_{200} cases on the x-axis are +50, +100, +150, and +200, respectively. Moreover, the origin point on the X-axis denotes the tunnel initial location.

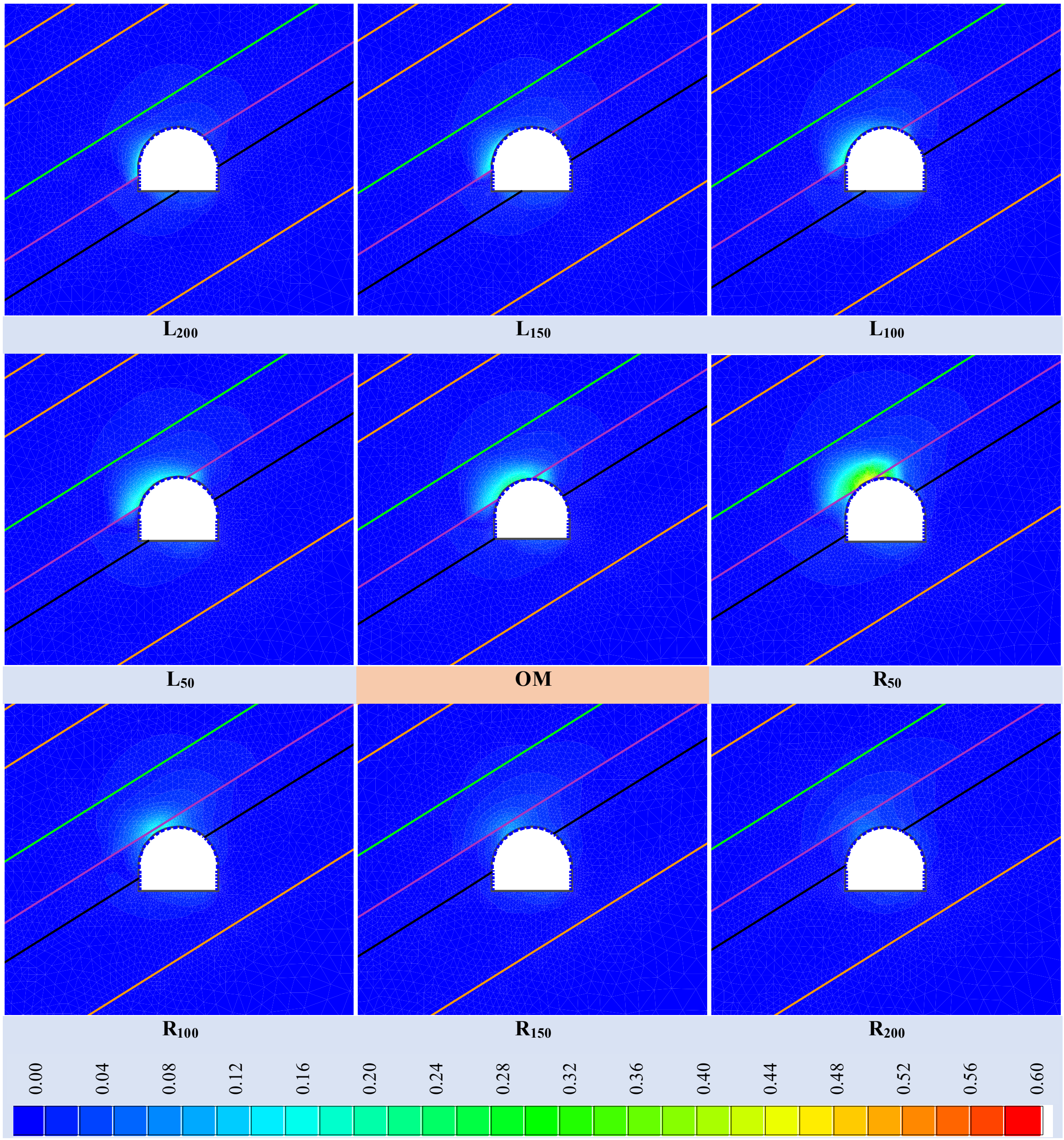

Figure 7. Contour-plot of absolute vertical displacements around tunnel induced by excavation for different tunnel horizontal locations relative to OM reference section.

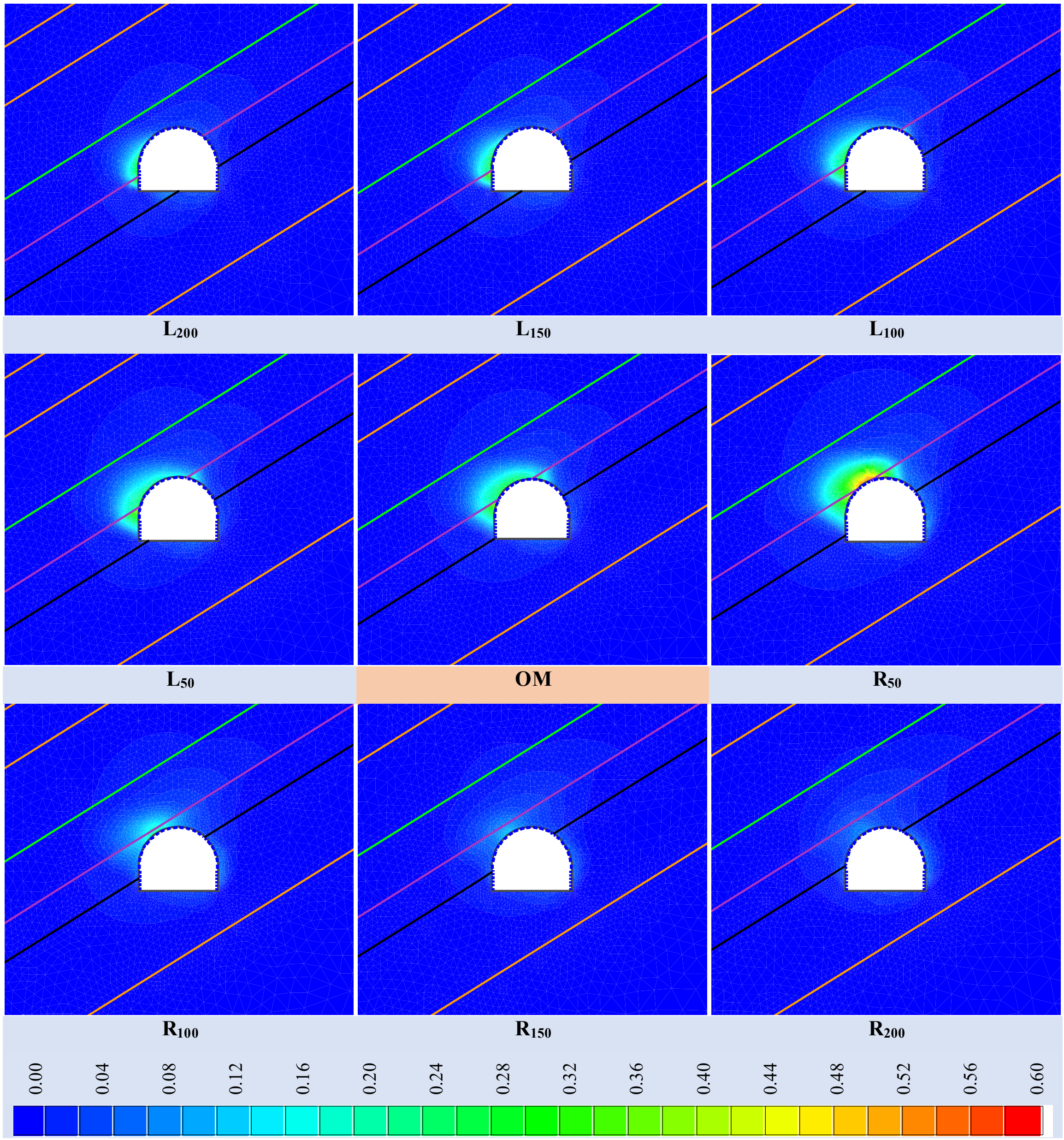

Figure 8. Contour-plot of total displacements around tunnel induced by excavation for different tunnel horizontal locations relative to OM reference section.

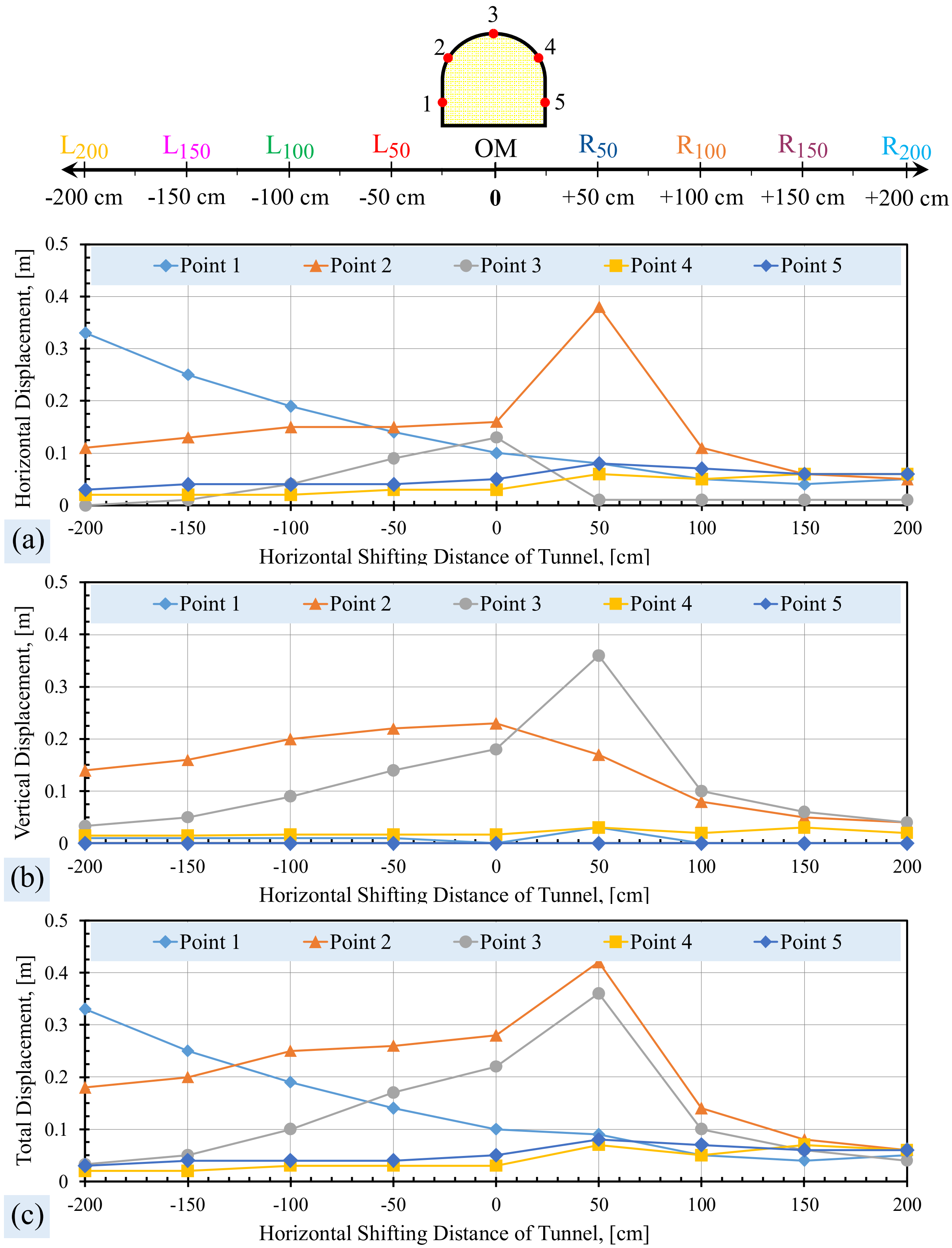

Figure 9. Variation of components of excavation induced displacement on the observation points: a) absolute horizontal, b) absolute vertical, and c) total displacement.

The first observation that can be inferred from Fig. 9 concerns the relationship between displacement components induced by tunnel excavation. At observation points 1, 4, and 5, the dominant component is horizontal displacement, which accounts for the majority of the total displacement induced by tunnel excavation. At these points, the other displacement components have a negligible effect on the total displacement. At other observation points, the relationship between the induced displacement components varies. For example, at point 2, the horizontal displacement is lower than the vertical displacement for the L_{200}, L_{150}, L_{100}, L_{50}, and OM cases, while the opposite is true for the R_{50}, R_{100}, R_{150}, and R_{200} cases. At point 4, the vertical displacement is nearly twice that of the horizontal displacement for most tunnel locations. At point 3 (the crown of the tunnel), the vertical displacement induced by tunnel excavation is higher than the horizontal displacement. This difference becomes more pronounced for the R_{50} and R_{100} cases, where the vertical displacement becomes the dominant component.

According to Fig. 9, the horizontal movement of the tunnel location to the left and right sides results in variable induced displacements at most of the observation points. The graphs of induced displacement components show a semi-undulating pattern with rising and falling fluctuations for all observation points except for point 1. The magnitude of horizontal and total displacements at point 1 continuously decreases as the horizontal shifting of the tunnel increases from L_{200} to R_{200}. Point 1 is located at the intercalary stone layer for all the tunnel horizontal movement cases, and its horizontal distance to the coal layer (the weakest layer in the domain) increases linearly as the tunnel shifts from L_{200} to R_{200}. This is the primary reason for the decreasing horizontal and total displacements at point 1. It is worth noting that the effect of increasing the horizontal thickness of this point to the coal layer gradually decreases, resulting in a further reduction of horizontal and total displacements at point 1.

According to Fig. 9, the displacement components for point 2 exhibit an ascending-descending variation, with a peak value at R_{50} and OM. Initially, this point is located in the coal layer for cases from L_{200} to OM, and moves to the intercalary stone layer with further rightward tunnel shifting. As the tunnel is shifted from L_{200} to OM, the thickness of the coal layer increases linearly in the direction normal to the tunnel boundary, causing an increase in the horizontal and vertical displacements induced by excavation. At R_{50}, point 2 is situated on the interface of the coal-intercalary layers, where the numerical modeling results indicate the maximum horizontal and total displacements. Upon further rightward tunnel shifting from R_{50} to R_{200}, the distance between point 2 and the coal layer (i.e. the thickness of the intercalary layer between the point and coal layer) increases linearly, leading to decreasing displacements.

According to Fig. 9, point 3 is located on the crown of the tunnel, where rightward horizontal shifting of the tunnel changes the host layer from coal to intercalary strata. The host strata for this point are coal and intercalary stone for L_{xx} and R_{xx} cases, respectively. Furthermore, this point is positioned on the interface of the coal-intercalary stone layers at OM. For all numerical models, the vertical displacement at this point is greater than the horizontal displacement. The induced displacement components exhibit a sudden change in rate of variation and magnitude for the R_{50} case. In this case, a singular zone forms above the tunnel crown, playing a special role in the distribution of displacement around the tunnel. The effect of this zone can also be observed in the contour plots of vertical and total displacement (Figs. 7 and 8). The zone is formed between the tunnel boundary and the coal-intercalary interface line. The effect of the zone disappears upon rightward tunnel shifting (R_{100}, R_{150}, and R_{200} cases) where the coal-intercalary interface line does not intersect the tunnel boundary.

Figure 9 illustrates that shifting the tunnel location to the left resulted in a variation of displacement components at most observational points. The rate of change in displacement components varies from point to point, depending on the placement of points in different layers. Points 2 and 3 initially located in the coal layer exhibit more variation in displacement rate than other points, as transmitting the tunnel to the left results in a decrease in the effective thickness of the coal layer above the tunnel. This leads to an intense decrease in total displacement at these points. In contrast, points 4 and 5 located in the sandstone and intercalary layers, respectively, do not exhibit tangible displacement rate changes with respect to shifting the tunnel location, as they remain in the same layers. The displacement pattern of point 1 is completely different from that of other points, due to its special location relative to the intercalary and coal layers. The variation in numerical model results at observational points indicates how the arrangement of strata with the tunnel boundary and the location of the intersection of weak strata with the tunnel control the distribution of induced displacements around the tunnel.

5. Conclusions

This paper focused on the effect of inclined strata on the excavation-induced displacements around a typical mine development tunnel driven along a coal seam. The main objective of this study was to evaluate the impact of the tunnel's location relative to the host ground strata, particularly the coal and weak intercalary layers.

To achieve the research objective, the numerical modelling of tunnel and host strata was performed through finite element analysis. At the first step, the numerical model was calibrated based on the field monitoring results of displacement. Then the calibrated model was used to investigate the effect of the horizontal location of the tunnel on the induced displacement field through sensitivity analysis. Finally, the results of sensitivity analysis on the tunnel's horizontal location were compared in terms of displacement components around the tunnel. Based on the presented results, the following conclusions were obtained:

- The calibrated numerical model demonstrates practical accuracy, with the maximum displacement ratio of the calibrated model to the measured values by monitoring being 0.84, 0.98, and 0.93 for three reference points. These values correspond to errors of 16%, 2%, and 7%, respectively, indicating the calibrated numerical model's accuracy for practical engineering purposes.
- Both horizontal and vertical displacements induced by excavation show asymmetric spatial distribution around the tunnel. The anisotropy of rock mass due to the inclined layers reasons the asymmetric spatial distribution of excavation-induced displacements. Additionally, the arrangement of weak-strength coal and intercalary stone strata relative to the tunnel excavation line plays a key role in the asymmetric spatial distribution of excavation-induced horizontal, vertical, and total displacements.
- The induced displacements are spatially concentrated in the intersection area of coal-intercalary stone interface with the tunnel excavation line. The spatial location of these weak rock strata relative to the tunnel boundary controls the magnitude, shape, and spatial distribution of induced displacements around the tunnel. Therefore, the magnitude and spatial spread of the induced total displacement decrease when the effect of these weak strata decreases. Such conditions arise by increasing the distances of weak strata (coal and intercalary stone) from the tunnel boundary or by decreasing the cut area of weak layers by the tunnel's internal surfaces.
- The critical state of stability or displacement around the tunnel is defined where displacement magnitude and spatial spread reach the maximum values. The critical state occurs when the intersection line of the coal-intercalary stone is tangent to the tunnel excavation line. The maximum displacement also occurs at the tangent point of the intersection line of coal-intercalary and the tunnel boundary. The excavation-induced displacement decreases by disclosing the intersection line of coal-intercalary stone from the tunnel.
- Comparison between results of numerical models for different tunnel horizontal locations relative to host rock mass layers indicates that the arrangement of strata with the tunnel boundary, the distances of weak layers to the tunnel, and the location of the intersection of weak strata with the tunnel are the most important factors affecting the distribution of displacement around the tunnel.

References

[1]. Zhuo, X., Liu, X., Shi, X., Liang, L., & Xiong, J. (2022). The anisotropic mechanical characteristics of layered rocks under numerical simulation. *Journal of Petroleum Exploration and Production Technology*, *12*(1), 51-62.

[2]. Zhang, Z. X., Xu, Y., Kulatilake, P. H. S. W., & Huang, X. (2012). Physical model test and numerical analysis on the behavior of stratified rock masses during underground excavation. *International Journal of Rock Mechanics and Mining Sciences*, *49*, 134-147.

[3]. Hoek, E., Carranza-Torres, C., Diederichs, M. S., & Corkum, B. (2008, February). Integration of geotechnical and structural design in tunnelling. In *Proceedings University of Minnesota 56th Annual Geotechnical Engineering Conference* (Vol. 29, pp. 1-53). Minneapolis.

[4]. Fortsakis, P., Nikas, K., Marinos, V., & Marinos, P. (2012). Anisotropic behaviour of stratified rock masses in tunnelling. *Engineering Geology*, *141*, 74-83.

[5]. Hoek, E., Marinos, P. G., & Marinos, V. P. (2005). Characterisation and engineering properties of tectonically undisturbed but lithologically varied sedimentary rock masses. *International Journal of Rock Mechanics and Mining Sciences*, *42*(2), 277-285.

[6]. Cheng, L., Wang, H., Chang, X., Chen, Y., Xu, F., Zhang, B., & An, J. (2021). Experimental study on the anisotropy of layered rock mass under triaxial conditions. *Advances in Civil Engineering*, *2021*, 1-13.

[7]. Tavallali, A., & Vervoort, A. (2010). Effect of layer orientation on the failure of layered sandstone under Brazilian test conditions. *International journal of rock mechanics and mining sciences*, *47*(2), 313-322.

[8]. Tien, Y. M., Kuo, M. C., & Juang, C. H. (2006). An experimental investigation of the failure mechanism of simulated transversely isotropic rocks. *International journal of rock mechanics and mining sciences*, *43*(8), 1163-1181.

[9]. Diederichs, M. S., & Kaiser, P. K. (1999). Stability of large excavations in laminated hard rock masses: the voussoir analogue revisited. *International Journal of Rock Mechanics and Mining Sciences*, *36*(1), 97-117.

[10]. Evans, W. (1941). The strength of undermined strata. *Transactions of the Institutions of Mining and Metallurgy*, *50*, 475-500.

[11]. Li, Y. (2019). Analytical examination for the stability of a competent stratum and implications for longwall coal mining. *Energy Science & Engineering*, *7*(2), 469-477.

[12]. Shabanimashcool, M., & Li, C. C. (2015). Analytical approaches for studying the stability of laminated roof strata. *International Journal of Rock Mechanics and Mining Sciences*, *79*, 99-108.

[13]. Sofianos, A. I. (1996, February). Analysis and design of an underground hard rock voussoir beam roof. In *International journal of rock mechanics and mining sciences & geomechanics abstracts* (Vol. 33, No. 2, pp. 153-166). Pergamon.

[14]. Yiouta-Mitra, P., & Sofianos, A. I. (2018). Multi-jointed stratified hard rock roof analysis and design. *International Journal of Rock Mechanics and Mining Sciences*, *106*, 96-108.

[15]. Cai, M., Morioka, H., Kaiser, P. K., Tasaka, Y., Kurose, H., Minami, M., & Maejima, T. (2007). Back-analysis of rock mass strength parameters using AE monitoring data. *International Journal of Rock Mechanics and Mining Sciences*, *44*(4), 538-549.

[16]. Li, A., Liu, Y., Dai, F., Liu, K., & Wang, K. (2022). Deformation mechanisms of sidewall in layered rock strata dipping steeply against the inner space of large underground powerhouse cavern. *Tunnelling and Underground Space Technology*, *120*, 104305.

[17]. Nehrii, S., Sakhno, S., Sakhno, I., & Nehrii, T. (2018). Analyzing kinetics of deformation of boundary rocks of mine workings. *Mining of mineral deposits*, (12, Iss. 4), 115-123.

[18]. Chen, H. (1993). Failure Modes of Mine Tunnels in Stratified Rock Structures with Reference to Stress Field Conditions. *Proceedings of 12th International Conference on Ground Control in Mining.*

[19]. He, M. (2011). Physical modeling of an underground roadway excavation in geologically 45 inclined rock using infrared thermography. *Engineering Geology*, *121*(3-4), 165-176.

[20]. He, M., Jia, X., Gong, W., & Faramarzi, L. (2010). Physical modeling of an underground roadway excavation in vertically stratified rock using infrared thermography. *International Journal of Rock Mechanics and Mining Sciences*, *47*(7), 1212-1221.

[21]. Nehrii, S., Nehrii, T., Zolotarova, O., Aben, K., & Yussupov, K. (2021). Determination of the parameters of local reinforced zones under the protection means. In *E3S Web of Conferences* (Vol. 280, p. 08018). EDP Sciences.

[22]. Sun, X., Zhao, C., Zhang, Y., Chen, F., Zhang, S., & Zhang, K. (2021). Physical model test and numerical simulation on the failure mechanism of the roadway in layered soft rocks. *International Journal of Mining Science and Technology*, *31*(2), 291-302.

[23]. Alejano, L. R., Taboada, J., García-Bastante, F., & Rodriguez, P. (2008). Multi-approach back-analysis of a roof bed collapse in a mining room excavated in stratified rock. *International Journal of Rock Mechanics and Mining Sciences*, *45*(6), 899-913.

[24]. Cai, M. (2008). Influence of stress path on tunnel excavation response–Numerical tool selection and modeling strategy. *Tunnelling and Underground Space Technology*, *23*(6), 618-628.

[25]. Do, N. A., Dias, D., Tran, T. T., Dao, V. D., & Nguyen, P. N. (2019). Behavior of noncircular tunnels excavated in stratified rock masses–Case of underground coal mines. *Journal of Rock Mechanics and Geotechnical Engineering*, *11*(1), 99-110.

[26]. He, B., Zhang, Z., & Chen, Y. (2012). Unsymmetrical load effect of geologically inclined bedding strata on tunnels of passenger dedicated lines. *Journal of Modern Transportation*, *20*, 24-30.

[27]. Zhang, Z. X., Xu, Y., Kulatilake, P. H. S. W., & Huang, X. (2012). Physical model test and numerical analysis on the behavior of stratified rock masses during underground excavation. *International Journal of Rock Mechanics and Mining Sciences*, *49*, 134-147.

[28]. Tsesarsky, M., & Hatzor, Y. H. (2006). Tunnel roof deflection in blocky rock masses as a function of joint spacing and friction–a parametric study using discontinuous deformation analysis (DDA). *Tunnelling and Underground Space Technology*, *21*(1), 29-45.

[29]. Winn, K., Wong, L. N. Y., & Alejano, L. R. (2019). Multi-approach stability analyses of large caverns excavated in low-angled bedded sedimentary rock masses in Singapore. *Engineering Geology*, *259*, 105164.

[30]. Yang, X. X., Jing, H. W., & Qiao, W. G. (2018). Numerical investigation of the failure mechanism of transversely isotropic rocks with a particle flow modeling method. *Processes*, *6*(9), 171.

[31]. Yaylaci, M. (2022). Simulate of edge and an internal crack problem and estimation of stress intensity factor through finite element method. *Advances in nano research*, *12*(4), 405.

[32]. Yaylaci, M., ADIYAMAN, G., Oner, E., & Birinci, A. (2021). Investigation of continuous and discontinuous contact cases in the contact mechanics of graded materials using analytical method and FEM. *Computers and Concrete*, *27*(3).

[33]. Zhang, X., Yang, J., & Chen, J. (2009). Stability Analysis of Tunnel Driven in Stratified Anisotropic Rockmass. In *Recent Advancement in Soil Behavior, in Situ Test Methods, Pile Foundations, and Tunneling: Selected Papers from the 2009 GeoHunan International Conference* (pp. 237-242).

[34]. RocScience Incorporated 2023, *RocScience*, https://www.rocscience.com.

[35]. Małkowski, P. (2015). The impact of the physical model selection and rock mass stratification on the results of numerical calculations of the state of rock mass deformation around the roadways. *Tunnelling and Underground Space Technology*, *50*, 365-375.

[36]. Martin, C. D., Kaiser, P. K., & McCreath, D. R. (1999). Hoek-Brown parameters for predicting the depth of brittle failure around tunnels. *Canadian Geotechnical Journal*, *36*(1), 136-151.

[37]. Bieniawski, Z. T. (1978, October). Determining rock mass deformability: experience from case histories. In *International journal of rock mechanics and mining sciences & geomechanics abstracts* (Vol. 15, No. 5, pp. 237-247). Pergamon.

[38]. Dinc, O. S., Sonmez, H., Tunusluoglu, C., & Kasapoglu, K. E. (2011). A new general empirical approach for the prediction of rock mass strengths of soft to hard rock masses. *International Journal of Rock Mechanics and Mining Sciences*, *48*(4), 650-665.

[39]. Hoek, E., & Diederichs, M. S. (2006). Empirical estimation of rock mass modulus. *International journal of rock mechanics and mining sciences*, *43*(2), 203-215.

[40]. Barton, N. R. (1972, September). A model study of rock-joint deformation. In *International Journal of Rock Mechanics and Mining Sciences & Geomechanics Abstracts* (Vol. 9, No. 5, pp. 579-582). Pergamon.

[41]. Goodman, R. E. (1991). *Introduction to rock mechanics*. John Wiley & Sons.

[42]. Potts, D. M., Zdravković, L., Addenbrooke, T. I., Higgins, K. G., & Kovačević, N. (2001). *Finite element analysis in geotechnical engineering: application* (Vol. 2). London: Thomas Telford.

[43]. Hoek, E., Carranza-Torres, C., & Corkum, B. (2002). Hoek-Brown failure criterion-2002 edition. *Proceedings of NARMS-Tac*, *1*(1), 267-273.

[44]. Barton, N., & Bandis, S. (1990). Review of predictive capabilities of JRC-JCS model in engineering practice. *In Proceedings of the Rock Joints-Proceeding of a Regional Conference of the International Society for Rock Mechanics, Loen,* pp. 603–610.

تاثیر جانمایی تونل نسبت به لایه‌های شیب‌دار زغال سنگ بر جابجایی‌های ناشی از حفاری: کاربرد مدل عددی کالیبره شده

مرتضی جوادی اصطهباناتی[۱*]، اشکان شاه‌پسند[۱]، شهربانو صیادی[۲]، و آرش شاه‌پسند[۳]

۱. دانشکده مهندسی معدن، نفت و ژئوفیزیک، دانشگاه صنعتی شاهرود، شاهرود، ایران
۲. دانشکده مهندسی معدن، دانشگاه صنعتی اصفهان، اصفهان، ایران
۳. بخش مهندسی معدن، دانشگاه آزاد اسلامی واحد علوم و تحقیقات، تهران، ایران

ارسال ۲۰۲۳/۰۱/۱۵، پذیرش ۲۰۲۳/۰۸/۱۴

* نویسنده مسئول مکاتبات: mortezjavadi@gmail.com

چکیده:

توده سنگ لایه‌ای – رسوبی معمول ترین زمین میزبان تونل‌های معدنی زغال‌سنگ بوده که به دلیل وجود سطوح لایه بندی (سطوح ناپیوستگی با طول بسیار زیاد) با رفتار آنیزوتروپ در معدن کاری زغال شناخته می‌شوند. در مطالعه حاضر، تاثیر جانمایی یک تونل دنبال لایه نسبت به موقعیت لایه‌های مختلف سنگ میزبان (لایه‌های شیب‌دار) بر روی جابجایی‌های ناشی از حفر تونل مورد بررسی قرار گرفته است. برای رسیدن به این هدف، ابتدا یک مدل عددی المان محدود (FEM) کالیبره شده مبتنی بر جابجایی‌های حاصل از رفتارنگاری برای یک تونل معدنی زغال‌سنگ در عمق ۳۰۰ متر توسعه داده شد. در ادامه، بررسی اثر جانمایی افقی تونل بر میدان جابجایی القایی با این مدل عددی کالیبره شده در قالب تحلیل حساسیت مورد ارزیابی قرار گرفت. در نهایت، نتایج تحلیل حساسیت از نظر مولفه‌های مختلف جابجایی در اطراف تونل مورد مقایسه قرار گرفت. نتایج این مطالعه نشان می‌دهد که مدل عددی کالیبره شده، با خطای میانگین حدود ۸ درصد برای بیشینه جابجایی در نقاط اندازه‌گیری شده، دارای دقت مناسبی برای کاربردهای عملی است. تحلیل‌های عددی نشان می‌دهند که به دلیل ناهمسانگردی توده سنگ میزبان تونل (به ویژه در لایه‌های شیبدار) توزیع فضایی جابجایی‌های اطراف تونل کاملا به صورت نامتقارن است. همچنین، چیدمان لایه‌های زغال‌سنگ و میان لایه‌های بسیار ضعیف نسبت به خط حفاری تونل نقش کلیدی در عدم تقارن جابجایی‌های اطراف تونل دارد. حالت بحرانی جابجایی‌ها (حداکثر جابجایی در تحلیل حساسیت) در حالتی رخ می‌دهد که خط تلاقی زغال‌سنگ و میان لایه‌های ضعیف با خط حفاری تونل مماس باشد. همچنین، با افزایش فاصله بین سطح مشترک لایه زغال‌سنگ (و میان لایه های ضعیف اطراف آن) و خط حفاری تونل، میزان جابجایی‌های القایی کاهش یافته که مقدار کمینه ۱/۵ متر برای این فاصله برای کاربردهای عملی پیشنهاد می‌شود.

کلمات کلیدی: توده سنگ لایه‌ای، معدن زغال‌سنگ، مدل عددی، کالیبراسیون مبتنی بر رفتارنگاری، جابجایی‌های نامتقارن، جانمایی تونل.